**33RD CONGRESS
OF THE INTERNATIONAL COUNCIL
OF THE AERONAUTICAL SCIENCES
STOCKHOLM, SWEDEN, 4–9 SEPTEMBER, 2022**

ICAS 2022 SWEDEN

Experimental Investigations on Tensile Properties of Aluminum Honeycomb Sandwich Structures with Single-sided Repairing

Bing Yan[1,2], Guijia Zhang, Mingbo Tong[1*], Lei Li[1], Dingchang Yu[1], Shuhua Zhu[1], Zhangyu Wu[3], Hao Wang[4], Tao Jin[5]

[1]Key Laboratory of Fundamental Science for National Defense Department of Aircraft Design, Nanjing University of Aeronautics & Astronautics, Nanjing, 210016, PRC
[2]DEMec, Faculdade de Engenharia, Universidade do Porto, Rua Dr. Roberto Frias, s/n, Porto, 4200-465, Portugal
[3]Department of Civil and Airport Engineering, Civil Aviation College, Nanjing University of Aeronautics and Astronautics, Nanjing, 210016, China
[4]College of Material Science and Technology, Nanjing University of Aeronautics and Astronautics, Nanjing, 210016, China
[5]China Special Vehicle Research Institute, Jingmen 448035, Hubei, P. R. China

Abstract

Tensile properties of single-sided panel repair(SP) and panel/core repair(SPC) of aluminum alloy honeycomb sandwich structure(AAHSS) used in civil aircraft were researched by experiments and compared with that of AAHSS without repair. Firstly, a clamp suitable for testing the tensile properties of wide-wall panels with different thicknesses was designed. Then, the failure behavior, the strain and deformation characteristics of SP and SPC structures were firstly studied by digital image correlation (DIC) technology. The results showed that the debonding of the patch and the fracture near the root were the main failure modes of the SP structure, and the strength recovery rate was 101%. A summary was that the repairing method for this configuration could effectively improve the bearing capacity of the original structure, and the adhesive performance was more stable. For SPC structure, debonding of the patch was the primary failure mode with only a 94% strength recovery rate. Besides, the strain concentration of both repairing structures was located in the substrate near the upper and lower edges of the patch. It can be concluded that the repairing technology of SP structure is sufficient to be used in civil aircraft repair, while that of SPC structure needs to be further improved.

Keywords: aluminum honeycomb sandwich structures, bonding repair, tensile properties, digital image correlation, strain distribution characteristics

1. Introduction

The metal honeycomb sandwich structure is widely used in civil aircraft, not only because of its excellent mechanical properties, but also compared with composite honeycomb sandwich structure, it can better resist ozone and ultraviolet damage to aircraft components. For example, aluminum honeycomb sandwich structures are used in the wingtips, spoilers, and other structures of B737NG aircraft [1]. However, civil aircraft are often used in various harsh climates, which causes defects in aluminum honeycomb sandwich structures such as debonding, corrosion, and pits. The mechanical properties of the damaged parts decrease sharply, which can affect the flight performance directly [2]. Replacing the whole damaged structures is not an economical, time-saving method, so it is necessary to repair damaged parts to restore the strength and efficiency of structures. According to the Structural Repair Manual(SRM) [1], when the degree of damage reaches the specified damage allowable range, the structure needs to be repaired in time.

The most traditional repairing method for aircraft structure is mechanical connection repair [3,4]. However, this method will dramatically increase the weight of the original structure, the sealing

performance and aerodynamic shape of the structure will be also influenced, and severe stress concentration will be caused around the joint holes. These disadvantages make the application of bonding repairing method development rapidly [5]. From geometrical considerations, bonding repairs are usually divided into bilateral (symmetric) and single-sided (asymmetric) repairing. Although the out-of-plane displacement caused by reinforcement which usually occurs in single-sided repairing structures may reduce the repair efficiency, usually only one side of the structure such as the fuselage or wing of aircraft can be reached in realistic repairing, which makes the single-sided repairing method much more popular in actual repair.

Today, the application of polymer matrix composite (PMC) patches to repair damaged structures is common in industries due to the high specific modulus, strength, and high flexibility [6-10]. It is also justifiable to repair cracked structure with composite patches, which is certificated by researchers in their studies [11-13]. This type of patch does not increase the weight of the structure [13] and can increase the fatigue lifetime of the part [15,16]. In US air force and aerospace industries, composite patches have been used as reinforcements to repair aircraft's damaged metal structures [17] and welcomed due to the high yield and economic efficiency [18]. However, special mounting equipments and complicated repairing methods are needed in using composite patches; simultaneously, the desired strength recovery capability of the repaired structure cannot be achieved due to various problems [19]. Firstly, lacking resistance against heat, moisture, and corrosion [20], the composite patch is not suitable to repair structures using in the harsh environment. Secondly, residual thermal stresses, the essential factor in reducing the repaired structure's strength recovery rate, are induced by the difference in thermal expansion coefficient between the substrate and the patch [21]. Besides, the strength recovery rate of the structure after bonding repair largely depends on the quality of bonding, and the bonding strength between composite and metal is much lower than that of metal and metal [22]. Electrical corrosion is prone to occur between the composite patch and the metal structure, making this method not suitable for long-term repair. In conclusion, it is still the first choice to repair metal structures to use the same material as the substrate as the repair reinforcement.

Many scholars used the finite element analysis method to study the stress characteristics and strain distribution of structures [23, 24]. However, the original structures may be simplified and idealized, which cannot fully reflect the real stress characteristics. Digital image correlation(DIC) technology, a practical and useful measurement tool to observe the full-field strain distribution information and displacement field of the specimen directly, has been widely recognized and used in the field of experimental mechanics in recent years [25-27]. Compared with the traditional strain gauge measurement method, the specimens' mechanical properties are not affected by DIC technology. Also, DIC technology can meet the measurement requirements of extensive deformation tests and eliminate the uncertainty factors caused by the strain concentration area. Therefore, DIC technology is used as the primary strain measurement method in this paper.

Most of the research on aircraft structure repair is focused on the repair technology of composite patch and the mechanical properties of repairing structures [2,23], the research on the mechanical properties of repairing structure with the metal patch is still relatively few. In this work, the mechanical properties of single-sided panel repair(SP) and single-sided panel/core repair(SPC) of aluminum alloy honeycomb sandwich structure(AAHSS) were studied by experiments, where the same aluminum alloy to the substrate was used for the patch. In addition, the strain distribution and deformation characteristics of repairing structures under tensile load were observed comprehensively by DIC technology, which provided experimental support for the stress and deformation analysis of repaired components on aircraft structures. Another highlight of this paper is that a clamp suitable for testing the tensile properties of wide-wall panels with different thicknesses was designed, which can overcome the problem that the wide-wall panels cannot be directly loaded by an existing test machine.

2. Materials and clamping scheme

2.1 Specimens

The tensile properties of bonding repair of AAHSS structure were tested in three groups, including Non-destructive structure(NS), single-sided panel repair(SP) structure, and single-sided panel/core repair(SPC) structure. The test matrix and dimension information are shown in Table 1. 2024-T3

aluminum alloy was the material of substrate and patch, respectively. ZMS1588 aluminum honeycomb was used as the material for making honeycomb core.

Table 1 The test matrix of repairing structures

Type	Numbering	Number of cases	Damage diameter r /mm	Size of specimen (Length×Width)/mm2	Hight of core/mm	The thickness of reinforcing and panel/mm	The diameter of reinforcing/ mm
NS	NS-X	6					
SP	SP-X	17	50.4	250×600	12.7	0.5	126
SPC	SPC-X	17					

The configuration of the SPC structure is shown in Figure 1. Firstly, the damaged part of the aluminum facesheet and honeycomb core (only the damaged part of the aluminum facesheet for single-sided panel repair) were completely removed from the substrate. Then, polyfoam was used to bond the repaired core and aluminum honeycomb core. Lastly, a small circle aluminum facesheet was glued onto the surface of the repaired core, and the patch was stick onto the entire repair area. The patch-attached side was called the repaired face, while another flat side was called the non-repaired face.
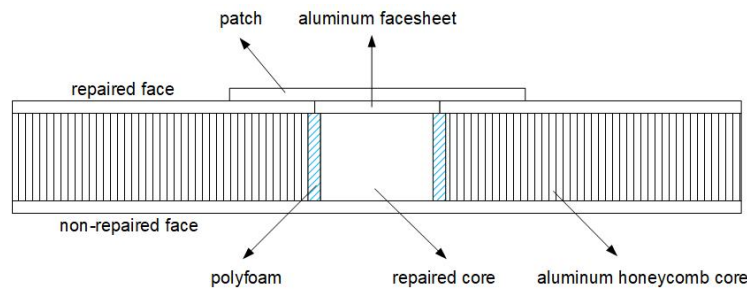
Figure 1 – The repairing method of SPC structure

2.2 The clamping scheme design of variable thickness wide-wall panels

The tests were carried out on the MTS Model 311.31 hydraulic servo fatigue testing machine, while the loading rate was 1mm/min. The clamp width ranges of the fatigue testing machine is between 90~130mm, so a directly clamping scheme was not adopted in the tensile tests of large size repaired structures under a large fracture load level. Aiming at testing the tensile properties of wide-wall panels with 250mm width and different thicknesses, a clamp was designed according to the manual [28]. The designed load was 30t, and the safety factor was 2. The clamp consisted of lugs, clamping sheets with hobbing teeth, and M10, M18, M38 bolts of grade 12.9, as shown in Figure 2, and the clamp was made of No.45 steel. The main design idea of the clamp was to increase the friction between the inner clamp and the ends of specimens by applying a large preload on the clamp by bolts, which to simulate the loading of the machine clamp more realistically. The load applied by the testing machine was transferred to the specimen mainly through friction, and the bolts bear little or no shear load in the loading process. Uneven loading and severe stress concentration caused by the hole at patch were prevented effectively, which may result in section fracture near the ends. The even distribution of load in the working section can be verified by back-to-back strain data and DIC technology, respectively.

Figure 2 – The clamping scheme of the sample

2.3 Strain measurement

Pasting strain gauges on the face of the specimen is a traditional strain measurement method. This method, which requires time-consuming pre-experimental operations and professional patch techniques, can only measure strain in a certain direction at one point. In contrast, the distribution of full-field strain and displacement can be observed directly by DIC technology. In this section, a comparative test between the two measuring methods was done. In this article, the two methods were both used for measurement.

Figure 3 showed the results measured by DIC technology. The full-field strain and displacement distribution can be observed directly, and all the result information of a point during the loading process can also be output directly by the computer. For the traditional method, the arrangement and numbering of gauges were drawn in Figure 4. The numbering in parentheses (e.g. (1-3), (2-2)) indicated that the strain gauges were attached to the non-repaired face of the specimen, others attached to the repaired face. The strain gauges numbered 1-1, 1-2, and 1-3 were set to demonstrate the loading uniformity of the fixture designed in section 2.2.
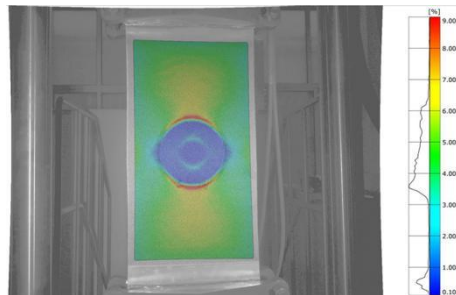
Figure 3 – Full-field longitudinal strain plot as measured by DIC
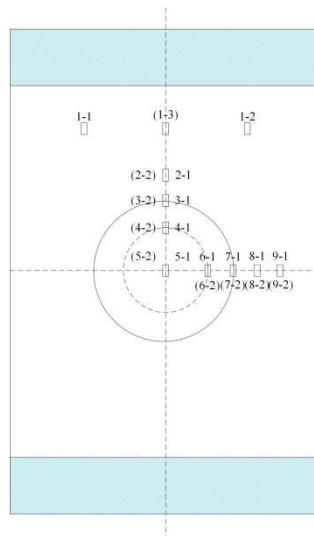
Figure 4 – Distribution of strain measurement

For the same point on the surface of the specimen, the strain-time curve of gauge numbered (1-1) was in good agreement with that measured by DIC, as shown in Figure 5, which makes valid points about the relative convenience and value of DIC over traditional strain gages.
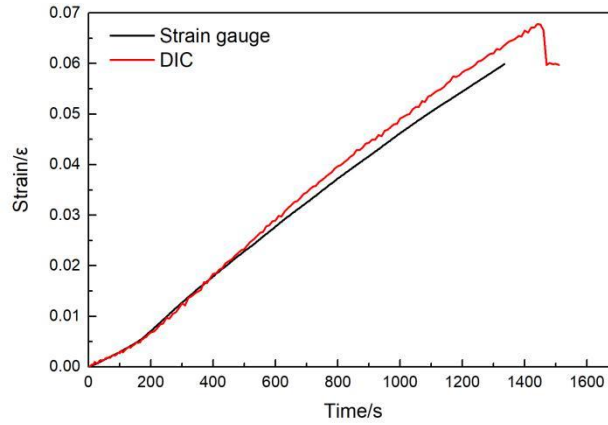
Figure 5 – Comparison between the results of DIC technology and strain gauges

3. Results and discussion

3.1 The relationship of stress-average strain

The stress-strain curves of NS, SP, and SPC structures are shown in Figure 6. The average strain in the working section of the specimen increased linearly during the initial loading stage. When the tensile yield strength of the aluminum alloy material (about 330MPa) was reached, the slope decreased obviously and the load increased slowly. For non-destructive specimens, failure occurred when the average strain of the specimen was higher than 0.045ε (Figure 6(a)). For SP structure, failure may occur when the strain was higher than 0.035ε (Figure 6(b)), and the dispersion coefficient of debonding strain was 11.49%, which indicated the adhesive performance was stable. For the SPC structure, the debonding failure occurred randomly once the applying load was over the critical yield point (Figure 6(c)), and the dispersion coefficient of debonding strain was 30.41%, which can prove the quality of bonding between the substrate and patch was poor. The failure strain level of SP and SPC structures depended on the adhesive quality, such as initial defects, bonding area, and adhesive thickness. In addition, more initial defects such as air bubbles and weak bonding may exist in the seam of the honeycomb of SPC structures, so it is easier to produce debonding failure than the SP structures at a low load level.
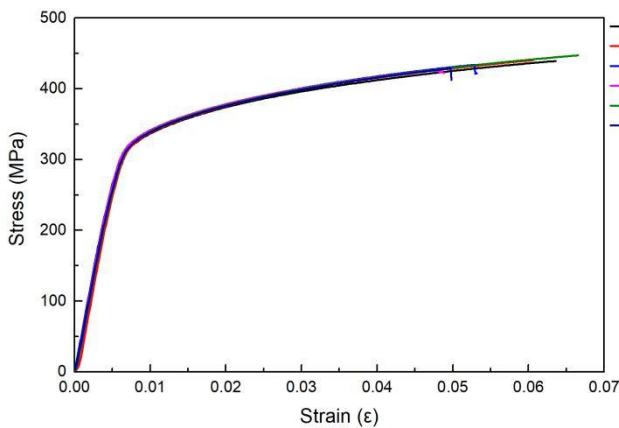
(a)Non-destructive specimens(NS)
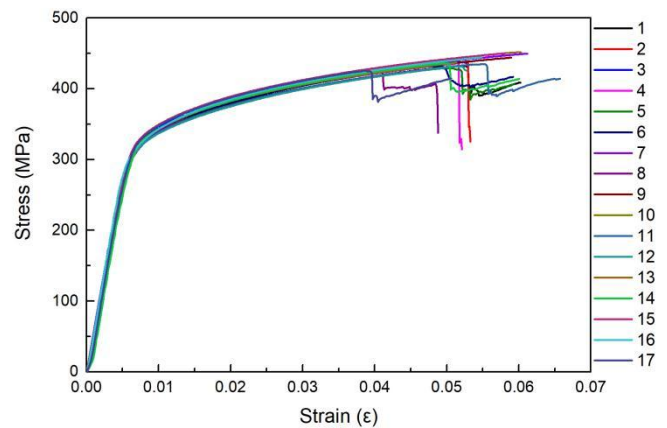
(b) Specimens with single-sided panel repair(SP)
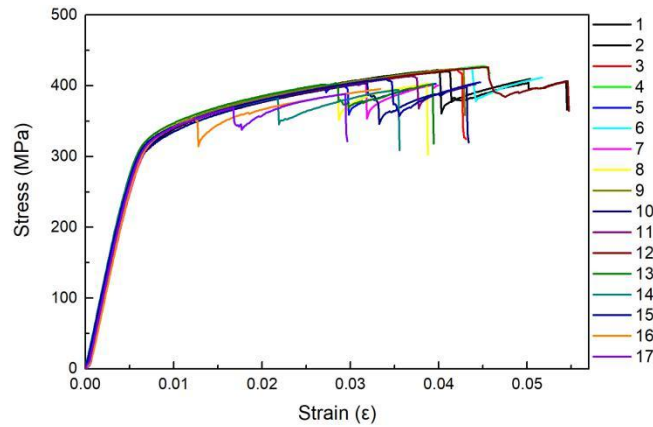
(c) Specimens with panel/core repair(SPC)

Figure 6 – The stress-strain curves of three type specimens

During the loading process, the first load drop caused by the debonding of the patch was named as the debonding load, and the final load drop was named as the fracture load. The failure load of the structures can be defined as the first load drop. The average values of failure strength are shown in the last column of Table 2, and the data in parentheses are dispersion coefficients of results. The average failure strength of NS specimens was 430.69MPa. The average failure strength of the SP specimens was 437.12MPa with a 101% strength recovery rate, which means this repairing method can restore the load-bearing capacity of damaged structures to the strength of original structures. The average failure strength of the SPC specimens was 406.66MPa, and the strength recovery rate can reach 94%.

Table 2 The failure mode and results

type	Failure mode	Percentage of failure modes	Debonding strength (MPa)	Debonding strain(ε)	Fracture strength (MPa)	Fracture strain(ε)	Failure strength (MPa)
NS	B	100%	—	—	431 (2.64%)	0.057 (11.08%)	431 (2.64%)
SP	A1	41.18%	430 (1.23%)	0.047 (11.49%)	411 (1.12%)	0.058 (9.46%)	437 (1.95%)
	A2	17.65%	—	—	442 (1.53%)	0.055 (6.73%)	
	B	41.18%	—	—	442 (1.43%)	0.055 (6.87%)	
SPC	A1	88.23%	403 (5.08%)	0.032 (30.41%)	402 (1.47%)	0.043 (17.19%)	407 (5.04%)
	A2	5.88%	—	—	424	—	
	B	5.88%	—	—	428	—	

3.2 Failure mode

The failure mode of different types of specimens can be divided into three categories. The first category was abbreviated as failure mode A1, the damage propagation process of which including the debonding of the patch and the cross-sectional fracture in the repairing area, as shown in Figure 7. Firstly, the debonding occurred at the adhesive of longitudinal upper and lower edges of reinforcing where the shear stress and peeling stress of adhesive reached the largest value, and the load suddenly dropped for the first time, as shown in Figure 7(a). Then, the debonding gradually expanded around the repairing panel to the entire repairing area, and the bearing capacity increased slightly. Finally, the bearing capacity was entirely lost due to the large area debonding and the hole at the center of the repairing area, as shown in Figure 7(b)(c). The second failure mode was abbreviated as A2. This kind of failure mode also fractured in the repairing area, but it is different from A1, as shown in Figure 8. The fracture occurred near the longitudinal upper

and lower edges of reinforcing without debonding process, which means that the bonding between reinforcing and the substrate was solid. In addition, there was a transverse dent at the corresponding position of the patch on the non-repaired face during the loading process, this can be attributed to the severe stress concentration caused by the plastic bending at the substrate near to the longitudinal upper and lower edges of the patch. The third failure mode was the root fracture that occurred at the joint of epoxy resin sealant and honeycomb sandwich, which was abbreviated as B. As is shown in Figure 9, the ultimate strength of the material had been reached.

(a)Initial debonding	(b)Propagation of the debonding	(c)Failure mode on non-repaired face

Figure 7 – The damage propagation process of failure mode A1

Figure 8 – The damage propagation process of failure mode A2   Figure 9 – Failure mode B

All the tests results are summarized in Table 2. For non-destructive honeycomb structures, B was the only failure mode. For SP structure, all failure modes existed, and mode A1 had the same probability of occurrence with mode B, which was 41.18%, and mode A2 occupied only 17.65 %. For SPC structure, mode A1 was the primary failure mode, which accounted for 88.24%. Only 2/17 specimens exhibited A2 and B failure modes, respectively.

For the structures with failure mode A1, it can be found from Table 2 that the structure still had load-bearing capacity in the stage of average strain increase 0.011ε after debonding. For SP structure with failure mode A1, the strength recovery rate was 100%, which had reached the strength of NS structure and indicated the reinforcing effect of the patch. However, the strength recovery rate of the SPC structure with the failure mode A1 was 93%, which was significantly lower than that of the SP structure. This phenomenon can be attributed to poor bonding quality caused by initial defects, such as air bubbles, in the repairing area and the seam of the honeycomb.

For the SP structure with the failure modes A2 or B, there was little difference in the fracture strength and fracture strain of the two failure modes, and the strength recovery rate of both were more than 100%, which also showed the reinforcing effect of the patch. For SPC structures with failure modes A2 or B, the fracture strength of the two failure modes is similar, and both are slightly smaller than the NS structure. However, further studies are needed before general conclusions can be drawn due to the small sample size.

3.3 Deformation analysis of metal honeycomb repairing structure

In this section, the longitudinal of the metal honeycomb repairing structure under tensile load was detailed studied mainly by DIC technology. For a comprehensive analysis, sufficient specimens were selected from NS, SP and SPC structures to measure the longitudinal strain by gauges, which compared with the longitudinal strain measured by DIC technology.

For NS structures, the longitudinal strain's growth trend at different positions of both faces was the same during the loading process, as shown in Figure 10. The strain was 0.006ε when the panel's average strength reached the yield strength (330MPa) of the aluminum alloy material, after that the strain increased sharply. The strain distribution characteristics of the SP and SPC repairing structures were very different from NS structure. However, the strain distribution characteristics of the SP and SPC repairing structures measured by gauges and DIC technology were almost the same, which means that the effect of the polyfoam used in the honeycomb seam was very small and can be ignored. Besides, different failure modes had almost no effect on the strain distribution characteristics during loading. Therefore, typical specimens were selected below to analyze the full-field strain and deformation characteristics of the metal honeycomb repairing structure under tensile load.
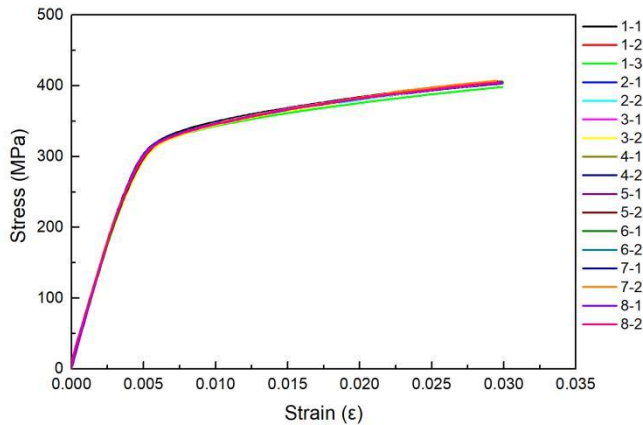
Figure 10 – The strain-stress curves of NS structure
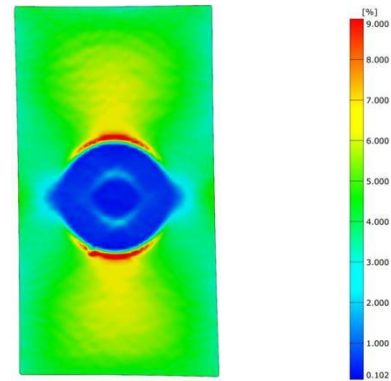
Figure 11 – The longitudinal strain distribution of repaired face

3.3.1 Strain distribution characteristics of repaired face

The typical specimen SP-13 with the failure mode B was selected. At the beginning of loading (about 60kN), the strain of the patch in the repairing area was slightly smaller than that of the substrate, and the low strain area of the patch was circular. As the load increased, the low strain area of the patch changed from a circle to an eye shape, as shown in Figure 11. At this time, the substrate on both sides of the patch was also in a low strain state due to the reinforcing effect of the patch, indicating that the patch can restrain the damaged area from being deformed and damaged. In addition, the maximum strain was located on the substrate near the upper and lower edges of the patch. The area of the strain concentration decreased as the load increased. The shape of the strain concentration area became a red crescent shape surrounding the patch when the specimen was about to fail. This was the weak place where the repairing specimen was most easily damaged under tensile load and was the stress concentration area on the entire structure of the repairing face. In addition to bearing the tensile load, it also borne the peeling stress applied by the adhesive layer.

The stress-strain curves recorded by strain gauges of the repairing face are shown in Figure 12. The strain on the substrate of the repairing surface was represented by the dot line, and the strain on the patch was noted by the solid line. It can be seen that the strain on the substrate increased faster as the load increased, which was significantly higher than the strain on the patch. However, 4-1 gauge in strain-load curves was significantly higher than the strain at the other locations of the patch, and slightly smaller than the strain on the substrate. The phenomenon was consistent with the result measured by DIC technology. As shown in Figure 13, the local strain distribution nephogram of patch at the later stage of loading was recorded by DIC technology, and the crescent-shaped red area was the place corresponding to 4-1 gauge. The load transferring in the repairing area was very complicated, where involved the transmission path of load at the overlap of the substrate, the patch and the repairing panel. The cross-sectional area of the three overlaps was the smallest, so the strain here was the largest.
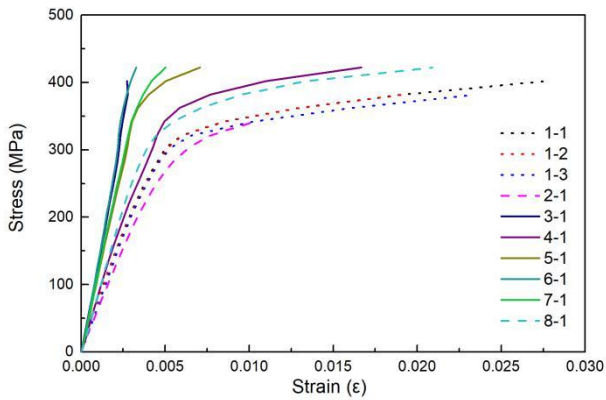
Figure 12 – The strain-load curves of repaired face
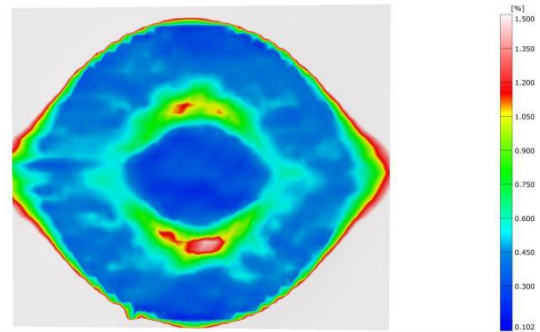
Figure 13 – Local longitudinal strain distribution in reinforcing face

3.3.2 Strain distribution characteristics of the non-repaired face

The typical specimen SP-11 with the failure mode B was selected to analyze the strain distribution characteristics, which were basically the same as the strain distribution characteristics of the repaired face. The difference was the shape of the low strain area like a diamond, as shown in Figure 14. At the beginning of the load process, the highest strain of the substrate was near the four corners of the rhombus on the non-repaired face. The low strain in the repairing area on the non-repaired face was evident before the failure load, and the location of strain concentration occurred on the substrate near the longitudinal upper and lower edges of the repaired area.
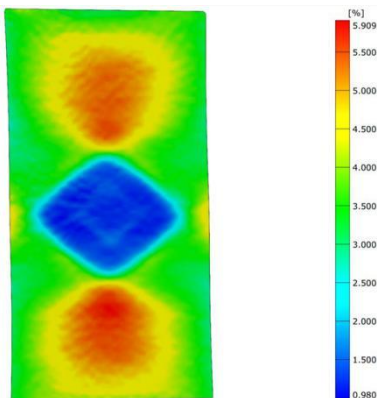
Figure 14 – The longitudinal strain distribution of non-repaired face
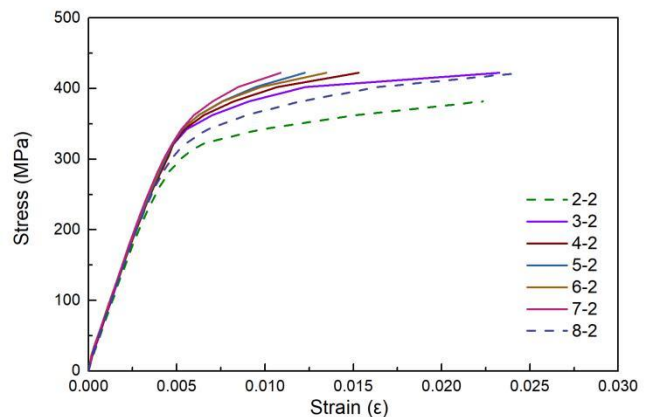
Figure 15 – The strain-load curves of non-repaired face

The stress-strain curves of the non-repaired face recorded by strain gauges are shown in Figure 15. When the load was at a low level, the strain in the non-repaired area at different positions increased linearly and the growth slope was almost the same. When the load increased to about 65kN, the strain corresponding to the repairing area began to be smaller than that of the substrate, which was especially obvious when the specimen was about to fail. In addition, the strain in the repairing area of the non-repaired face increased from the center of reinforcing area to the edge of that, which was consistent with the results of DIC technology. The local strain distribution nephogram of the non-repaired face was shown in Figure 16. It can also be seen that the strain in the area where was the overlap of the substrate, the patch and the repairing panel was higher than the surrounding area in the repairing area. This phenomenon occurred in the SP and the SPC repairing structures. Therefore, for a metal honeycomb one-side repair structure of this thickness, the structural characteristics of the repair surface can also affect the strain distribution of the non-repair surface.
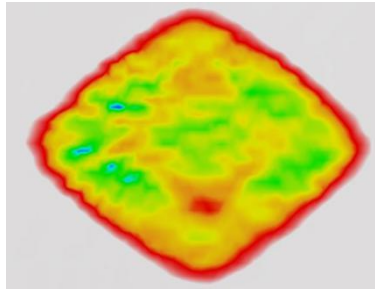
Figure 16 – Local longitudinal strain distribution in non-repaired face

3.3.3 Comparative analysis of strain characteristic on repaired face and non-repaired face

The stress-strain curves of the gauges at the patch on the repaired face and non-repaired face were shown in Figure 17. It can be observed that, except for the 4-X strain gauges, the strain in the repaired area of the repaired face was significantly lower than that of the non-repaired face.

The stress-strain curves of the strain gauges on the repaired face and the non-repaired face on the substrate were shown in Figure 18. It can be concluded that the strain measured by the back-to-back strain gauges on repaired face and non-repaired face was almost the same throughout the loading process.
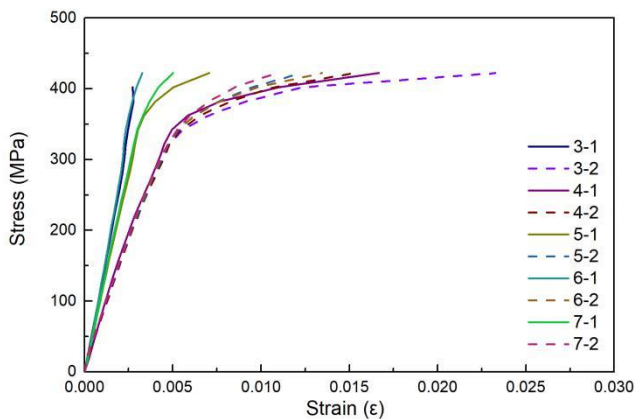
Figure 17 – Strain comparative of repaired face and non-repaired face on patch
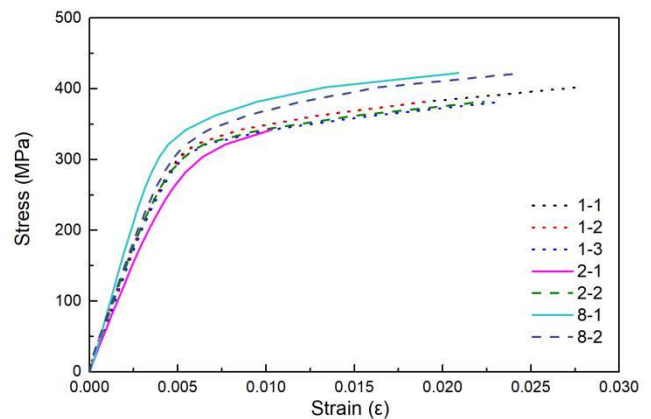
Figure 18 – Strain comparative of repaired face and non-repaired face on the substrate

4. Conclusions

The failure behavior and deformation characteristics of non-destructive structure(NS), single-sided panel repaired(SP) structure and single-sided panel/core repair(SPC) structure was studied by experiments. Based on the reported results, significant conclusions can be summarized as following:

Firstly, a clamp is designed to test the tensile properties of wide-wall panels with different thicknesses, which proves that the idea of applying load by the friction produced by bolt preload is feasible. The test results of the fixture are reasonable and practical.

Secondly, the failure mode of single-sided panel repair(SP) and single-sided panel/core repair(SPC) of AAHSS under tensile load can be divided into three categories, including the fracture in the repaired area caused by debonding, fracture in the substrate near to the upper and lower edges of patch caused by high shear stress and peeling stress of adhesive layer, and root fracture near the joint of epoxy resin sealant and honeycomb sandwich. For the SP structure, this repairing method has an excellent repair effect. Debonding and root fracture are the primary failure mode, and the failure strength recovery rate is 101%. For the SPC structure, debonding is the primary failure mode, and the failure strength recovery rate only reaches 93%. Besides, it means poor and unstable bonding quality that the higher dispersion coefficient of the failure strength recovery rate is 30.41%. This can be mainly attributed to the more initial defects (such as air bubbles) in the repaired area and in the honeycomb seam of the SPC structure, which need to be improved by others repairing methods.

Lastly, the strain distribution characteristics of SP and SPC structure under tensile are the same. The longitudinal strain level of the repaired area is lower than that of the substrate due to the reinforcing

effect of the patch. For repaired face, strain concentration area is located at substrate around the upper and lower edges of patch where bearing tensile force and peeling stress applied by the adhesive at the same time. For the non-repaired face, the location of strain concentration is on the substrate near the upper and lower edges of the patch. In addition, for the repaired area, the strain level in the area where the substrate, the patch and the repaired panel overlap are the highest whether it is repaired face or non-repaired face. Compared with the strain of repaired area on the non-repaired face, the strain on the repaired face is significantly lower.

5. Acknowledgements

6. Copyright Issues

The authors declare that they have no conflicts of interest to this work. We declare that we do not have any commercial or associative interest that represents a conflict of interest in connection with the work submitted

7. Contact Author Email Address

The contact author:

Bing Yan: yanbing@nuaa.edu.cn

Mingbo Tong: tongw@nuaa.edu.cn

8. Copyright Statement

The authors confirm that they, and/or their company or organization, hold copyright on all of the original material included in this paper. The authors also confirm that they have obtained permission, from the copyright holder of any third party material included in this paper, to publish it as part of their paper. The authors confirm that they give permission, or have obtained permission from the copyright holder of this paper, for the publication and distribution of this paper as part of the ICAS proceedings or as individual off-prints from the proceedings.

References

[1] Structural repair manual[M]. Aircraft technical publishers, 2001.

[2] King, W.T., et al., Effects of honeycomb core damage on the performance of composite sandwich structures. Journal of Composite Materials, 2020. 54(16): p. 2159-2171.

[3] ARMSTRONG K B, GRAHAM BEVAN L, COLE II W F. Care and repair of advanced composites[M]. 2nd ed. Warrendale: SAE International, 2005: 258-266.

[4] Galińska, A., Mechanical Joining of Fibre Reinforced Polymer Composites to Metals—A Review. Part I: Bolted Joining. Polymers, 2020. 12(10): p. 2252.

[5] FLYNN B W, B.J.B.D., Advance technology composite fuselage-Repair and damage assessment supporting maintenance NASA-CR-473.

[6] W. Oudad, B. B. Bachir, M. Belhouari, S. Touzain and X. Feaugas, Analysis of the plastic zone size ahead of repaired cracks with bonded composite patch of metallic aircraft structures, Computational Materials Science, 46 (4) (2009)950-954.

[7] M. Masood and A. R. Ghasemi, Modified couple stress theory and finite strain assumption for nonlinear free vibration and bending of micro/nanolaminated composite Euler- Bernoulli beam under thermal loading, Journal of Mechanical Engineering Science, 231 (21) (2017) 4044-4056.

[8] M. M. Attar, F. Barati, M. Ahmadpour and E. Rezapour, Failure analysis of unidirectional polymeric matrix composites with two serial pin loaded-holes, Journal of Mechanical Science and Technology, 30 (6) (2016) 2583-2591.

[9] H. Robati and M. M. Attar, Analytical study of a pinloaded hole in unidirectional laminated composites with triangular and circular fibers, Journal of Applied Mechanics, 80 (2)(2013) 021018.

[10] Liu, X., et al., Bonded Repair Optimization of Cracked Aluminum Alloy Plate by Microwave Cured Carbon-Aramid Fiber/Epoxy Sandwich Composite Patch. Materials, 2019. 12(10): p. 1655.

[11] G. C. Tsai and S. B. Shen, Fatigue analysis of cracked thick aluminum plate bonded with composite patches, Compos. Struct., 64 (2004) 79-90.

[12] A. R. Ghasemi and K. Hosseinpour, Thermo-magneto- mechanical long-term creep behavior of three-phase nano- composite cylinder, Composites Science and Technology, 167 (2018) 71-78.

[13] A. R. Ghasemi, M. Mohandes, R. Dimitri and F. Tornabene, Agglomeration effects on the vibrations of CNTs/fiber/polymer/metal hybrid laminates cylindrical shell, Composites Part B, 167 (2019) 700-716.

[14] N. G. Tsouvalis, L. S. Mirisiotis and D. N. Dimou, Experimental and numerical study of the fatigue behaviour of composite patch reinforced cracked steel plates, Int. J. Fatigue., 31 (2009) 1613-1627.

[15] V. Sabelkin, S. Mall and J. B. Avram, Fatigue crack growth analysis of stiffened cracked panel repaired with bonded composite patch, Engng. Fract. Mech., 73 (2006) 1553-1567.

[16] M. M. Attar, Analytical study of two pin-loaded holes in unidirectional fiber-reinforced composites, Journal of Applied Mechanics, 80 (2) (2013) 021004.

[17] C. Okfar, N. Singh, U. E. Enemuoh and S. V. Rao, Design, analysis and performance of adhesively bonded composite patch repair of cracked aluminum aircraft panels, Compos. Struct., 71 (2005) 258-270.

[18] W. Y. Lee and J. J. Lee, Successive 3D FE analysis technique for characterization of fatigue crack growth behavior in composite-repaired aluminum plate, Compos. Struct., 66 (2004) 513-520.

[19] Dehghanpour, S., et al., Repairing cracked aluminum plates by aluminum patch using diffusion method. Journal of Mechanical Science and Technology, 2019. 33(10): p. 4735-4743.

[20] F. A. Ghasemi, A. Pourkamali and A. Roozbahani, Using XFEM for investigating the crack growth of cracked aluminum plates repaired with fiber metal laminate (FML) patches,Modares Mechanical Engineering, 13 (14) (2014) 15-27 (in Persian)

[21] A. R. Ghasemi, M. Mohammadi Fesharaki and M. Mohan- des, Three-phase micromechanical analysis of residual stresses in reinforced fiber by carbon nanotubes, Journal of Composite Materials, 51 (12) (2017) 1783-1794.

[22] Pitta, S., et al., On the static strength of aluminium and carbon fibre aircraft lap joint repairs. Composite Structures, 2018. 201: p. 276-290.

[23] Shen Q, Zhu Z, Liu Y. Progressive failure analysis of scarf-repaired composite laminate based on damage constitutive model[J]. Proceedings of the Institution of Mechanical Engineers Part L Journal of Materials Design & Applications, 2019:1464420716666400.

[24] Truong V H, Kwak B S, Roy R, et al. Cohesive zone method for failure analysis of scarf patch-repaired composite laminates under bending load[J]. Composite Structures, 2019, 222(AUG.):110895.1-110895.11.

[25] Ruan J K, Wang Q B, Zhao L Y, et al. Airship skin strain measurement based on adaptive digital image correlation[J]. Aerospace Systems, 2020, 3(28).

[26] Pan B, Qian K, Xie H, et al. TOPICAL REVIEW: Two-dimensional digital image correlation for in-plane displacement and strain measurement: a review[J]. Measurement Science & Technology, 2009,

20(6):152-154.

[27] Fathi A, Keller J H, Altstaedt V. Full-field shear analyses of sandwich core materials using Digital Image Correlation (DIC)[J]. Composites Part B, 2015, 70:156-166.

[28] Wen B C. Mechanical design manual[M]. Machinery Industry Press, 2010.